PERGAMON

Neural Networks 13 (2000) 571–588

Neural Networks

www.elsevier.com/locate/neunet

Visual cortical mechanisms of perceptual grouping: interacting layers, networks, columns, and maps

W.D. Ross[1], S. Grossberg*, E. Mingolla

Department of Cognitive and Neural Systems and Center for Adaptive Systems, Boston University, 677 Beacon Street, Boston, MA 02215, USA

Received 17 December 1999; accepted 3 May 2000

Abstract

The visual cortex has a laminar organization whose circuits form functional columns in cortical maps. How this laminar architecture supports visual percepts is not well understood. A neural model proposes how the laminar circuits of V1 and V2 generate perceptual groupings that maintain sensitivity to the contrasts and spatial organization of scenic cues. The model can decisively choose which groupings cohere and survive, even while balanced excitatory and inhibitory interactions preserve contrast-sensitive measures of local boundary likelihood or strength. In the model, excitatory inputs from lateral geniculate nucleus (LGN) activate layers 4 and 6 of V1. Layer 6 activates an on-center off-surround network of inputs to layer 4. Together these layer 4 inputs preserve analog sensitivity to LGN input contrasts. Layer 4 cells excite pyramidal cells in layer 2/3, which activate monosynaptic long-range horizontal excitatory connections between layer 2/3 pyramidal cells, and short-range disynaptic inhibitory connections mediated by smooth stellate cells. These interactions support inward perceptual grouping between two or more boundary inducers, but not outward grouping from a single inducer. These boundary signals feed back to layer 4 via the layer 6-to-4 on-center off-surround network. This *folded feedback* joins cells in different layers into functional columns while selecting winning groupings. Layer 6 in V1 also sends top-down signals to LGN using an on-center off-surround network, which suppresses LGN cells that do not receive feedback, while selecting, enhancing, and synchronizing activity of those that do. The model is used to simulate psychophysical and neurophysiological data about perceptual grouping, including various Gestalt grouping laws.

Keywords: Visual cortex; Perceptual grouping; Cortical layers; Cortical columns; Cortical maps; Cortical feedback; Illusory contours; V1; V2; Lateral geniculate nucleus

1. Introduction: cortical substrates of perceptual grouping

The laminar organization of the visual cortex supports interactions among local circuits that form functional columns, which are themselves organized in cortical maps (Hubel & Wiesel, 1977). Yet, how the structures of layer and column interact to generate visual percepts remains obscure. This article develops a neural model of how the interacting structures of laminae, columns, and maps cooperate to generate perceptual groupings. Preliminary reports of some of the present results have appeared in Grossberg, Mingolla and Ross (1997).

While perceptual groupings have long been studied as psychophysical phenomena, a full understanding of their causes depends on modeling the underlying neural mechanisms by which the brain organizes local image features into coherent groupings of scenic features. Crucial to the process of perceptual organization are the cortical circuits that convert retinogeniculate measures of local image contrast into representations of oriented boundaries in a context-sensitive way. Emergent boundary groupings efficiently represent object borders and surface contours in response to texture, shading and depth cues (Beck, Prazdny & Rosenfeld, 1983; Grossberg, 1994; Julesz, 1971; Polat & Sagi, 1994; Ramachandran & Nelson, 1976). The cortical model developed herein shows how the context-sensitivity of such perceived boundary groupings can be explained by the context-sensitivity of neuronal responses, notably their "non-classical" receptive field properties, which can, in turn, be traced to specific aspects of the organization of local circuits.

While the cortical circuits we analyze are involved in many aspects of perceptual grouping, including textural segmentation, "good continuation," and figure/ground

* Corresponding author. Tel.: +1-617-353-7858; fax: +1-617-353-7755.
E-mail address: steve@cns.bu.edu (S. Grossberg).
[1] Present address: Sensor Exploitation Group, MIT Lincoln Labs, Lexington, MA 02173-9108, USA.

0893-6080/00/$ - see front matter
PII: S0893-6080(00)00040-X

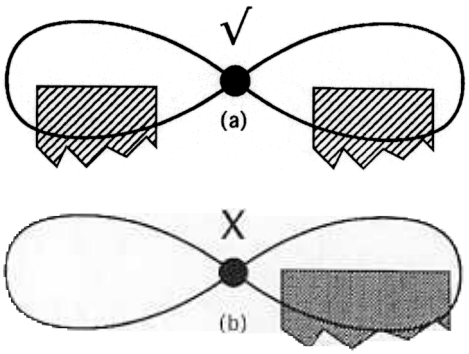

Fig. 1. A grouping cell can fire: (a) if it receives enough oriented, almost collinear input from both branches of its receptive field; but not (b) if it receives input from only one branch.

separation, illusory contours offer a particularly useful testbed for study. Illusory contours are instances of perceptual grouping because they are cases where disconnected local contrasts in a scene are linked together to form unbroken perceptual units. They are usually but not always perceptually sharp, typically support visible light/dark differences in abutting regions, and are often associated with perceived surface depth differences. (See Lesher, 1995 for a review.) While such striking perceptual effects may be absent in more prosaic forms of grouping, an important common mechanism unites the analysis of many perceptual phenomena in which percepts of continuous, elongated, and thin structures (i.e. contours) emerge from discrete scenic elements. To address such phenomena, Beck et al. (1983) refer to "linking", Field, Hayes and Hess (1993) invoke an "association field", and our work analyzes "cooperative bipole cells" (Gove, Grossberg & Mingolla, 1995; Grossberg, 1987; Grossberg & Mingolla, 1985).

To function effectively in perceptual contour formation or completion, a linking mechanism is required to possess a key computational characteristic: it must be activated whenever the receptive field of the mechanism is simultaneously stimulated on two sides by "bottom-up" input based on retinally registered contrasts, but *not* be activated whenever input, no matter how strong, is only registered on one side (see Fig. 1). We call this tendency "the bipole property." This property patently requires some form of non-linear computation, as the bipole must "decide" whether it is being stimulated by a sufficient number of units of activity on *each* side of its receptive field (e.g. five and five) to respond, or whether it is being stimulated only on one side (e.g. ten units) with no stimulation at all on the other, in which case it should not respond. Another way of stating the bipole property is to say that a bipole unit must *interpolate* a response supporting a perceptual contour if its receptive field center is located between two appropriately spaced inducing elements, but not *extrapolate* a perceptual contour away from a single isolated inducer.

The journey from a functional understanding of the bipole property to our present understanding of its instantiation in a detailed local-circuit model of V1 and V2 cell interactions has had to answer two difficult computational questions: first, *how can the "inward" logic of necessary and sufficient arrangements of inducers for perceptual interpolation be reconciled with the "outward" axonal connectivity patterns of long-range horizontal connections of visual cortex* (McGuire, Gilbert, Rivlin & Wiesel, 1991)? While a sketch of possible circuits for accomplishing this feat has already been provided (Grossberg et al., 1997), this article is the first to provide the equations of a model that addresses this issue.

The second key computational question addressed in this article concerns the reconciliation of: (a) the bipole property; (b) neural feedback circuits; and (c) the need for neural codes to assume a functional continuum of values (e.g. neural firing rates). Before even stating the question, however, some preliminary points must be clarified. To begin, the word "feedback" is used in several different senses in various scientific and technical communities. Before explaining the significance of feedback in our model, we must clarify that in using the term we refer to *any* "closed loop" of connectivity between neural units. Thus, "horizontal connectivity" whereby neuron A in a particular lamina of V1 synapses on neuron B of the same lamina, and where neuron B also synapses on neuron A, is the simplest possible example of nerve feedback. Such feedback is often referred to as "recurrent." Our model includes this form of feedback, as well as other forms. Some physiologists appear to reserve the word feedback to refer only to projections from a "later" cortical area to an earlier one (e.g. V2 to V1, or V1 to LGN). We prefer to describe the entire loop of such inter-area circuits, including both the "forward" and "backward" connections, as a feedback circuit, and the work presently reported includes such feedback. Finally, closed feedback loops can also be found *within* cortical areas, but involving cells of two or more laminae of a single area; we will discuss such feedback, and its relation to the other forms, at length.

The next point for clarification concerns the need for a near-continuum of possible output values in a neural code; we refer to this property as *analog sensitivity*. The percepts of many perceptual phenomena, including illusory contours, have been shown to be resolvable to rather fine gradations, using a variety of scaling techniques. (For a review, see Lesher, 1995.) That is, it is meaningful to speak of weak, or strong, illusory contours, or to reliably rank-order several illusory contour exemplars on dimensions such as clarity or brightness. Similarly, neural units in cortical areas have been shown to vary in response strength as a function of variables similar to those shown to affect perceptual response strength in humans (von der Heydt, Peterhans & Baumgartner, 1984). We assume that a causal connection exists between response rates of neural units in early cortical areas and perceptual response, and assert that any complete model of perceptual grouping, including illusory contour formation, must address how the *strength* of illusory contours can be represented along some analog dimension

of neural response. As will be seen, our model equations employ a lumped representation of neural potential, with a continuum of possible real-valued output signals, bounded above and below by saturation constants. These output signals may be viewed as proportional to firing rate in the output of more articulated equations for neural activity.

The second key computational question of our work can now be stated: *how can a neural feedback circuit both embody the bipole property and have analog sensitivity in its output values?* The case for using positive feedback to select the correct context-sensitive perceptual grouping is intuitively compelling (Grossberg & Mingolla, 1985), and we will describe the particular relevance of feedback to illusory contour formation later in this article. Moreover, positive feedback is not intrinsically incompatible with analog sensitivity in neural models. Since the work of Grossberg (1973), we have known that a suitable choice of feedback signal function (the transformation whereby the potential of one cell forms the signal that is transmitted as input to another cell), combined with a balance of excitatory and inhibitory connections, can guarantee analog sensitivity. It is the bipole property that, until recently, had thwarted modeling attempts at realizing robust analog-sensitive perceptual completion in feedback circuits. Without analog sensitivity, groupings formed at an early processing stage could easily lead to incorrect percepts and recognition events at higher processing stages.

The bipole property was first predicted based upon a psychophysical analysis (Cohen & Grossberg, 1984; Grossberg, 1984; Grossberg & Mingolla, 1985) at around the same time that it was reported in electrophysiological recordings from area V2 (von der Heydt et al., 1984). Until the simulations of Grossberg et al. (1997), however, no neural model had displayed analog sensitive behavior in a feedback circuit embodying the bipole property. Predecessors to the present model, including those of Gove et al. (1995) and Grossberg and Mingolla (1985), had displayed "all-or-none" contour completion. That is, if the model completed a contour at all between inducers, it would complete a contour of a certain strength, regardless of whether there were several strongly aligned inducers, or only the minimum set of inducers necessary to trigger completion.

For an intuitive understanding of the limitations of the predecessor model, consider that the bipole property was instantiated by certain simple non-linear transformations intended to create the type of "statistical and gate" required for perceptual interpolation without extrapolation (Grossberg & Mingolla, 1985). The model bipole cell was considered to have a two-lobed receptive field in the shape of a figure-eight. Recent research combining optical imaging of tree shrew cortex with biocytin injections has strikingly confirmed the hypothesis that cells which form long-range connections in cortex contact cells of similar orientational preference and that the receptive field centers of the contacted cells are aligned in the cortical map along directions that correspond to the orientational preference of the cell forming the axonal connection (Bosking et al., 1997; Schmidt, Goebel, Lowel & Singer, 1997). In the 1985 model, input signals arriving at each half of the figure-eight were separately subjected to saturating transformations. The transformations would map ever-increasing input values to the same "plateau" value, after an initial rising regime. The bipole cell would fire only if the sum of such transformed values from both sides of the figure-eight exceeded the maximum value attainable by inputs to just one side. While this step guaranteed interpolation without extrapolation, it also damaged the bipole's ability to reflect the strength of its input in the value of its output. (Recall that a bipole is "supposed" to fire if, say, inputs valued at 3 on a scale of 0–10 arrive on both sides, but not if an input valued at 8 is on one side, with an input of 0 on the other.) The combination of such bipole computations with feedback, however, guaranteed that the model system as a whole would converge to one of two possible values in a possible locus for an illusory contour. Either there would be completion (i.e. cells reaching a uniform positive output value) or not (i.e. cells at resting potential).

Intuitively, what was missing from the earlier model bipole computation was some procedure for assessing whether a certain alignment of inducing input elements was sufficient for completion of a contour *given the context of surrounding inputs.* Put another way, the completion signal needs to be scaled relative to the input signals, and the mechanism for determining *how strong* a completed contour signal should be needs to be buffered from the effects of the non-linear mechanism for deciding *whether* to complete a contour. Grossberg et al. (1997) sketched intuitively how to accomplish this feat, but that brief report contained no computational details of the key model mechanisms. The present article describes the laminar circuits of cortical areas V1 and V2 that compute analog groupings, the model equations that realize this property, simulations of psychophysical and neurophysiological grouping data, the dependence of model behavior on parameter choices, and additional model explanations of relevant data.

2. Methods

This section states the assumptions and linking hypotheses of the model and describe its core computational principles intuitively, for the sake of clarity. After presenting model equations and parameters, data simulations are described. Neurophysiological data that directly test the model architecture are described in the present section, while consideration of additional data that the model helps to explain is deferred Section 5.

Five computational properties comprise the core of the model. The description of these properties refers to the macrocircuit of the entire model shown in Fig. 2. This

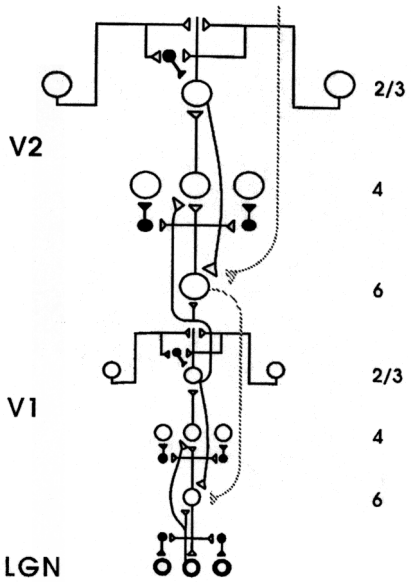

Fig. 2. Schematic of the entire model's circuitry, including LGN, V1, and V2 components. Open circles represent neurons, whether pyramidal cells in those layers labeled 2/3 or simple cells in layers labeled 4. Small dark circles represent inhibitory interneurons. The dark circles with light centers at the level labeled LGN stand for ON-center, OFF-surround cells. The model includes OFF-center, ON-surround cells as well, but these are not shown for simplicity. Triangles at the end of thin curves represent synapses. Open triangles represent excitatory synapses, and closed triangles represent inhibitory ones. The thin vertical line emanating from the center circle in the top layer (V2, 2/3) of the diagram represents a pyramidal cell's apical dendrite. A similar icon appears at the corresponding location at the V1 2/3 layer. The V2 circuit is proposed to be isomorphic to the V1 circuit, with all V2 cells having proportionately larger receptive fields than corresponding ones in V1. See the accompanying text for additional remarks on how to interpret this diagram. (Adapted with permission from Grossberg et al. (1997), Fig. 5).

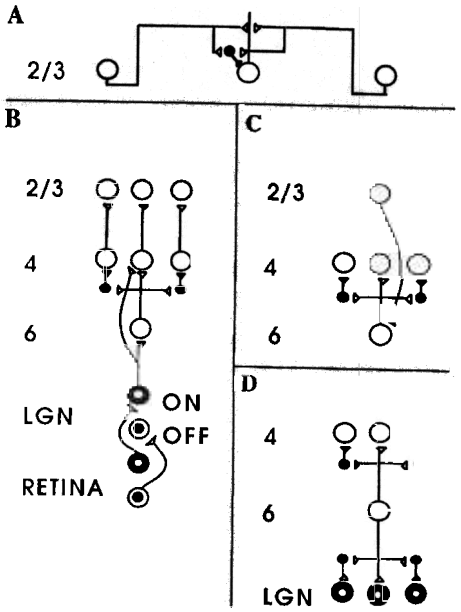

Fig. 3. Triangles at the end of thin curves represent synapses. Open triangles represent excitatory synapses, and closed triangles represent inhibitory ones. Model retinal, LGN and V1 circuit. (A) Horizontal bipole interactions in layer 2/3: layer 2/3 complex pyramidal cells monosynaptically excite one another via horizontal connections, primarily on their apical dendrites. They also inhibit one another via disynaptic inhibition that is mediated by model smooth stellate cells. Multiple horizontal connections are proposed to share a common pool of stellate cells near each target complex cell. The bipole property is hereby achieved. (B) Feedforward circuit from retina to LGN to cortical layers 4 and 6. Retina: retinal ON cells have an on-center off-surround organization. Retinal OFF cells have an off-center on-surround organization. LGN: the LGN ON and OFF cells receive feedforward ON and OFF cell inputs from the retina. Layer 4: layer 4C cells receive feedforward inputs from LGN and layer 6. LGN ON and OFF cell excitatory inputs to layer 4 establish oriented simple cell receptive fields. Layer 6 cells excite layer 4 cells with a narrow on-center and inhibit them from using layer 4 inhibitory interneurons, represented by small dark disks, that span a broader off-surround. Like-oriented layer 4 simple cells with opposite contrast polarities compete (not shown) before generating half-wave rectified outputs that converge on layer 2/3 complex cells. Layer 2/3: the converging simple cell outputs enable complex cells to respond to both polarities. They hereby full-wave rectify the image. (C) Cortical feedback loop from layer 2/3 to layer 6: layer 6 cells receive excitatory inputs from layer 2/3. The long-range cooperation hereby engages the feedforward layer 6-to-4 on-center off-surround network. This cooperative–competitive feedback loop can select winning groupings without a loss of analog-sensitivity. (D) Top-down corticogeniculate feedback from layer 6: LGN ON and OFF cells receive topographic excitatory feedback from layer 6, and more broadly distributed inhibitory feedback via LGN inhibitory interneurons that are excited by layer 6 signals. The feedback signals pool outputs over all cortical orientations and are delivered equally to ON and OFF cells. Corticogeniculate feedback selects, gain controls, and synchronizes LGN cells that are consistent with the cortical activation that they cause. Layer 6-to-4 inhibition and layer 6-to-LGN inhibition (mediated by inhibitory interneurons, represented by small dark disks) both contribute to length-sensitive (endstopped) responses that facilitate grouping perpendicular to line ends. (Adapted with permission from Grossberg et al. (1997), Fig. 3).

macrocircuit includes a number of simplifications of the model equations to highlight the essential components required for perceptual grouping. These circuits are next briefly described, so that the flow of neural signals in the model is clear. Supporting data and a description of the functional significance of the circuits are then provided.

The model's circuits include center–surround cells of LGN, which send excitatory signals to cells of layers 6 and 4 of V1, and receive inter-area feedback from layer 6 of V1. The feedback from layer 6 to LGN is modulated by a local center–surround circuit, indicated by three synaptic connections, two of which are to inhibitory interneurons, at the bottom of Fig. 3. Note also that the LGN to layer 4 pathway engages a similar center–surround circuit. Cells of layer 4 of V1 send excitatory signals to pyramidal cells in layer 2/3 of their own cortical column. These pyramidal cells are at the same time part of a horizontal feedback circuit formed with pyramidal cells with similar orientational preferences from nearby columns of layer 2/3. This feedback circuit also involves inhibitory interneurons.

That the intra-laminar connections of layer 2/3 form a lateral feedback circuit may not be evident from the icons of Fig. 2. This is because, for graphical simplicity, only a "minimal set" of existing connections is shown. For example, although only the middle cell (open circle) in layers 2/3 is shown as having an apical dendrite (vertical

line emanating from open circle), the others also have such structures, along with the corresponding synaptic connections and interneurons. Similarly, the center–surround circuits in layer 4 of V1 and the LGN, while only indicated by a single set of icons, are assumed to be replicated in an interdigitated way for all corresponding locations in the neural layers. Although the off-surround connections are assumed to be radially symmetric in the model, and to have a corresponding radial effect on cells' receptive fields, the horizontal circuits of layer 2/3 are assumed to preferentially link cells with similar orientational preference and whose receptive field centers are roughly aligned along the direction given by the cells' orientational preferences.

Besides processing inputs from layer 4 and engaging in recurrent feedback with neighbors, pyramidal cells of layers 2/3 also send excitatory signals, possibly via a polysynaptic route, to cells of layer 6 in retinotopically corresponding locations, that is, in their own cortical columns. Finally, we note that the structure of the model V2 circuit replicates its V1 circuit, but V2 cells are shown larger in the diagram in recognition of their larger receptive fields. The following sections provide an intuitive description of the model's key functional properties and how its circuits realize them computationally.

2.1. Property 1: boundary completion and grouping by bipole interactions among layer 2/3 pyramidal cells

According to the model, cooperative bipole interactions are achieved in layers 2/3 of V1 or V2 by recurrent long-range horizontal connections among cortical pyramidal cells. In order for cooperation to build a boundary like an illusory contour, monosynaptic excitatory connections from cells that are being driven by spatially separated retinal contrasts need to converge on the same pyramidal cell or cells. This class of pyramidal cells would thereby exhibit elongated and possibly figure-eight shaped receptive fields. The fanning out of the two lobes of the receptive field supports the possibility that perceptual completion or illusory contours can form along somewhat curvilinear, as opposed to only strictly collinear, paths. The horizontal synaptic connections also activate smooth stellate cells, which inhibit nearby pyramidal cells via disynaptic inhibition (Hirsch & Gilbert, 1991; McGuire et al., 1991). This disynaptic inhibition is proposed to modulate the effects of the monosynaptic excitation, and also to give rise to the bipole property, as follows.

Horizontal waves of activation propagating outwards from neurons driven by spatially isolated inducers are attenuated rapidly by subsequent disynaptic inhibition. It is a case of "one against one", in the sense that every unit of excitatory signal propagated outward is attenuated by a unit of inhibitory signal sufficient to negate the excitatory signal's effect, possibly after a brief temporal interval during which the earlier-arriving excitatory signal may transiently activate a recipient neuron. The important point is that the net amount propagating inhibition "supported by" a single isolated inducing contrast on the retina is sufficient to cancel the net amount of propagating excitation. This property is in accordance with studies showing that, when a single input source drives horizontal pathways at threshold intensities in vivo, excitatory postsynaptic potentials (EPSPs) are generated, whereas suprathreshold stimulus currents elicit disynaptic inhibitory postsynaptic potentials (IPSPs) that can overwhelm the EPSPs (Cannon & Fullenkamp, 1993; Hirsch & Gilbert, 1991; Knierim & van Essen, 1992; Somers, Nelson & Sur, 1995; Stemmler, Usher & Niebur, 1995). The perceptual correlate of this property is that grouping or illusory contour completion does not extrapolate, that is, propagate "outward" from a single inducing element.

Bipole completion occurs due to model interactions between monosynaptic excitation and disynaptic inhibition when layer 2/3 cells receive horizontally induced (i.e. intralaminar) activations from a surrounding neighborhood of cells with oriented receptive fields, and whose receptive field centers are displaced along the direction of orientational preference of the individual neurons (Grosof, Shapley & Hawkin, 1993; von der Heydt et al., 1984). The significance of disynaptic inhibition in our model is paramount. The interneuron receives excitatory signals from the same pyramidal cells of layers 2/3 that are attempting to activate a pyramidal neighbor. Its own synapse on that recipient pyramidal cell is inhibitory; this is the anatomy of "one against one" suppression of excitation by inhibition.

Convergent horizontal activations from both sides of the target cell can overcome the effect of disynaptic inhibition as follows. All the horizontal connections arriving in a cortical column are proposed to converge on a single population of inhibitory interneurons whose total activity is assumed to normalize or saturate (Fig. 3A). At the same time, a pyramidal cell is assumed to have a significantly higher saturation potential than the inhibitory interneurons when it receives excitatory inputs from both branches of its receptive field. The net effect on the target pyramidal cell is therefore excitatory; it is a case of "two (or more) against one." That is, multiple sources (two or more) of convergent input from *direct* pyramidal-to-pyramidal excitatory coupling can overcome the (one) source of *mediated* inhibition via the interneuron population. The outward propagating long-range horizontal signals from pyramidal cells are hereby converted into the selective inward activation of pyramidal cells according to a bipole property.

2.2. Property 2: analog sensitivity to LGN inputs through layers 6 and 4

The second design property suggests how V1 cortex preserves its contrast-sensitivity to signals from LGN, despite the non-linear processing required for bipole completion. As in the brain, inputs to the model area V1 arrive at layers 4 and 6 from the LGN (Hubel & Wiesel,

1962); see Fig. 3B. LGN inputs directly activate orientationally tuned simple cells in layer 4C. This property has been verified by cross-correlational analysis (Reid & Alonso, 1995) and by chemical and cooling inactivation experiments in the cortex (Chapman, Zahs & Stryker, 1991; Ferster, Chung & Wheat, 1996). Oriented arrays of spatially displaced LGN ON and OFF cells excite mutually inhibitory simple cells that are sensitive to the same orientation but opposite contrast polarities (Chapman et al., 1991; Ferster, 1988; Ferster et al., 1996). The LGN is proposed to indirectly excite and inhibit layer 4 via layer 6 using a short-range excitatory and longer-range inhibitory interaction that is mediated by layer 4 inhibitory interneurons. Electrophysiological recordings (Grieve & Sillito, 1991, 1995) and antidromic activation of layer 6 cells from the cat LGN (Ferster & Lindstrom, 1985) support the idea that layer 6 gives rise to a short-range excitatory input to layer 4 and a longer-range inhibitory interaction that is mediated by layer 4 inhibitory interneurons. The net effect is that LGN influences layer 4 via a feedforward on-center off-surround network. In the model, the cells in this network are proposed to obey membrane equations, or shunting laws (Hodgkin, 1964). Such a network preserves cell sensitivity to analog, or graded, input values even if absolute input amplitudes vary over a large dynamical range (Grossberg, 1973, 1980). It is critical to note that the property of analog sensitivity obtains *whatever* the source or sources of input; in particular, it is preserved when contour completion signals generated by the layer 2/3 bipole circuit join the "bottom-up" signals from LGN by feeding into layer 6 cells.

2.3. Property 3: folded feedback—interlaminar cortical circuits and functional columns

The third design property shows how the cortex makes double use of the layer 6-to-4 pathway to coherently select correct groupings, while suppressing incorrect ones, without a loss of analog sensitivity to the amount of contrast in inducing retinal signals. In particular, layer 4 cells activate pyramidal cells in layer 2/3, which then attempt to cooperate using their long-range horizontal connections and short-range disynaptic inhibition. All the layer 2/3 cells that become active either via direct layer 4 inputs or by bipole cooperation then generate excitatory feedback signals to layer 6 via layer 5 (Ferster & Lindstrom, 1983; Gilbert & Wiesel, 1979); see Fig. 3C. Layer 2/3 hereby gains access to the shunting on-center off-surround network from layer 6 to layer 4. The total interlaminar feedback loop proceeds through layers 4, 2/3, 5, 6, and 4. It converts the interacting cells throughout these layers into functional columns (Hubel & Wiesel, 1962, 1977; Mountcastle, 1957). The long-range cooperation in layer 2/3 can now use the shorter-range on-center off-surround network from layer 6 to 4 to selectively amplify those cell activations that are favored by the cooperative grouping, while suppressing those that are not, without eliminating their sensitivity to stimulus strength, notably to variable contrast (Grossberg, 1973), as has been shown in vivo (Douglas, Koch, Mahowald, Martin & Suarez, 1995).

Inhibition from layer 6 to layer 4 in the model influences different orientations and positions by being distributed across a cortical hypercolumn map where cells sensitive to these features are spatially organized (Blasdel, 1992a,b; Blasdel & Salama, 1986; Bonhoeffer & Grinvald, 1991; Grinvald, Lieke, Frostig & Hildesheim, 1994; Hubel & Wiesel, 1977; LeVay, Connolly, Houde & Van Essen, 1985; Lowel et al., 1987; Olson and Grossberg, 1988). This inhibition can relatively enhance cell responses that cooperate in positional, orientation, and length-sensitive groupings by suppressing those cells that respond to weaker groupings, incoherent noise, or background signals.

The pathways through layers 2/3, 5, 6, and 4, is called *folded feedback* (Grossberg, 1999) due to the way in which it folds the top-down feedback from layer 2/3 into the feedforward processing of bottom-up inputs to layer 4 (Fig. 3C), using the same layer 6-to-4 on-center off-surround network as the feedforward processing uses (Fig. 3B). The laminar structure of the cortical circuit makes such folded feedback possible. Folded feedback achieves two desirable modeling results. (1) It enables the output of the layer 2/3 recurrent bipole grouping circuit to be processed by the same network parameters as the feedforward inputs from LGN. This ensures that the strength of completion signals that indicate a set of inducers is "sufficiently close" or "sufficiently aligned" or "has sufficient contrast" to be grouped can be assessed relative to the sizes and distributions of the "bottom-up" signals from LGN generated by those same inducers. (2) The off-surround of the folded feedback circuit is well placed to selectively inhibit the influence of bottom-up LGN inputs at those locations which are not sufficiently supported by feedback from layer 2/3, thereby shutting down weaker groupings and preventing the propagation of perceptual "noise" to all subsequent stages of laminar cortical processing.

2.4. Property 4: corticogeniculate feedback

The fourth design property makes a third use of layer 6 processing. Layer 6 in both brain and model sends topographic excitation and broader-range inhibition back to the LGN (Murphy & Sillito, 1987, 1996; Weber, Kalil & Behan, 1989) see Fig. 3D. This feedback selects and amplifies LGN cell activities that are consistent with cortical cell activity, relative to those that are not. It carries out a type of top-down matching that increases signal-to-noise ratio by selectively attenuating LGN cells whose outputs do not succeed in activating, or maintaining activity in, cortical cells (McClurkin et al., 1994; Sillito et al., 1994). In summary, top-down feedback from cortical layer 2/3 to 6 uses the 6-to-4 pathway to shut down cortical cells in layer 4 whose outputs do not lead to strong layer 2/3 groupings. Layer 6-to-LGN feedback shuts down the inputs from

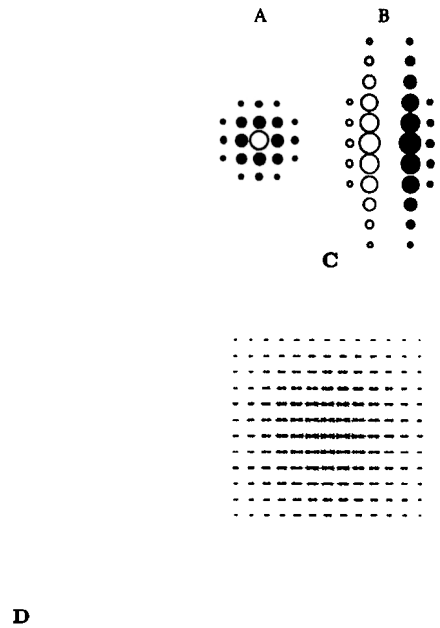

Fig. 4. Connectivity kernels: the size of the empty circles (filled circles) corresponds to the magnitude of positive (negative) connectivity values at a cell located at the center of the pattern. (A) Retinal center–surround connectivity. (B) Simple cell ON–OFF cell excitatory activation for a vertically oriented cell. (C) The spatio-orientational pattern of the layer 6-to-4 inhibitory surround connectivity. Superimposed at each location in the lattice are short line segments of up to 12 possible orientations, corresponding to the orientational preferences of cells of layer 4C. The length of each segment codes the weight of an inhibitory interaction from a cell of similar (in the case shown, horizontal) orientational preference, and whose receptive field center is displaced from the inhibited cell by the distance from a particular lattice location to the center. (D) V1 layer 2/3 oriented lateral excitatory connectivity for a horizontally oriented complex cell. (E) V2 layer 2/3 oriented lateral excitatory connectivity.

LGN cells to layer 4 cells that are not part of "winning" groupings. Layer 6 hereby seems to do triple duty in organizing feedforward inputs, intracortical feedback, and corticogeniculate feedback.

2.5. Property 5: similar organization at different scales of areas V1 and V2

The fifth design property implements data showing that cortical areas V1 and V2 (areas 17 and 18 in the cat) exhibit circuits with many homologous features, but V2 has longer-range interactions than V1 (Amir, Harel & Malach, 1993; see Fig. 2) Consistent with this idea, Kisvarday, Toth, Rausch and Eysel (1995) have presented a quantitative study of orientation maps (using multiunit recordings) and of cortical connections (using biocytin injections analyzed in horizontal sections) showing no significant differences in the proportions of excitatory and inhibitory cells and their preferred orientational contacts across areas V1 and V2, but did show a larger scale in V2 than V1. This property may be summarized by the hypothesis that the interblob circuits of V1 and the interstripe circuits of V2 have a similar organization. We propose that the V1 horizontal interactions help to organize the development of positional, orientational, and disparity tuning in this area, whereas the longer-range V2 interactions support long-range boundary completion and grouping across the blind spot, retinal veins, and textured scenes. As in the brain, layer 2/3 of the model V1 circuit activates layers 4 and 6 of the model V2 circuit (van Essen & Maunsell, 1983; Felleman & van Essen, 1991); see Fig. 2.

3. Model equations

Below are the equations and simulation methods that we used to develop and evaluate the model. Each section includes a discussion of how we chose parameters, including a description of where in the model parameters are robust and our understanding of the reasons for sensitivity of certain parameters. Tables list the values of all parameters used and Fig. 4 graphically depicts the important excitatory and inhibitory connectivity patterns (kernels) of the model. The reader can understand Section 4, in which data simulations are shown, without first reading these model equations.

3.1. General forms of model equations

Each neuron was modeled as a single voltage compartment in which the membrane potential was given by

$$C_m \frac{dV(t)}{dt} = -(V(t) - E_{EXCIT})g_{EXCIT}(t) - (V(t) - E_{INHIB})g_{INHIB}(t) - (V(t) - E_{LEAK})g_{LEAK}, \quad (1)$$

where the parameters E represent reversal potentials, g_{LEAK} is a constant leakage conductance, and the time-varying conductances $g_{EXCIT}(t)$ and $g_{INHIB}(t)$ represent the total inputs to the cell. Transient after hyperpolarization terms (AHP) were not incorporated since all groupings were allowed to reach steady state. For present purposes, layers of nerve cells (or cell populations) are denoted by their positions (i,j) in a rectangular array. These cells are influenced by excitatory E_{ij} and inhibitory I_{ij} inputs according to the membrane equation (1), now rewritten for the purposes of computational intuition in the form (Grossberg, 1973):

$$\frac{dW_{ij}}{dt} = -AW_{ij} + (B - W_{ij})E_{ij} - (C + W_{ij})I_{ij}. \quad (2)$$

In Eq. (2), a cell's "resting" activation is scaled to equal zero, and its potential can range from a positive value (B) to a negative value ($-C$, where C is a positive number). At equilibrium, each cell's activity can be expressed as a

Table 1
Cortical BCS parameters I

Name	Description	Value	Equation(s)
Stage I: V^R modeled retinal processing			
A	Activation decay rate	1.0	Retina shunt
B	Saturation level	1.0	Retina shunt
C	Hyperpolarization term	1.0	Retina shunt
σ_R	Retina surround standard deviation	1.2	6

biased difference-of-Gaussians (DOG) divided by a biased sum-of-Gaussians (SOG), due to the automatic gain control terms W_{ij} in Eq. (2) that multiply the inputs E_{ij} and I_{ij}. These equilibrium activities are half-wave rectified to generate output signals V_{ij}, namely,

$$V_{ij} = \left[\frac{BE_{ij} - CI_{ij}}{A + E_{ij} + I_{ij}}\right]^+, \tag{3}$$

where $[w]^+ = \max(w, 0)$ represents the half-wave rectification operation. The definitions of E_{ij} and I_{ij}, as well as the parameters A, B, and C for each level, are defined below. Throughout, two types of Gaussian kernels will be used to define receptive fields. Processing in the retinal and LGN stages of the model use unoriented, symmetric, normalized Gaussian kernels of the form:

$$G_{ij} = \frac{1}{\sigma\sqrt{2\pi}} \exp\left(-\frac{i^2 + j^2}{2\sigma}\right), \tag{4}$$

where (i,j) represent positional indices and σ represents the kernel's standard deviation. Cortical receptive fields typically use oriented, normalized Gaussian kernels of the form:

$$\exp\left\{-.5\left[\frac{i\cos\frac{k\pi}{12} - j\sin\frac{k\pi}{12}}{2\sigma_l}\right]^2 + \frac{(i + \text{offset})\cos\frac{k\pi}{12} + (j + \text{offset})\sin\frac{k\pi}{12}}{2\sigma_w}\right]^2\right\} \tag{5}$$

where (i,j) represent positional indices, k the orientation of the major axis of the oriented Gaussian distribution, and the σs represent standard deviations in the directions of receptive field length (l) and width (w). The factor "offset" specifies the displacement of Gaussians from the center of the receptive field of the unit described in Eq. (5).

We next describe the particular equations of each model layer in turn. The input image for a simulation is denoted by an array of input intensities S_{ij}. For our simulations, image sizes were 256 rows by 256 columns except for the "shifted grating" simulations, which were 128 × 128, and the intensities ranged from 0 to 255. All model layers representing cells with orientational selectivity had units tuned to 12 different orientations at each of the layer's 65,536 locations. In the following description of model stages, we do not explicitly write equations for a particular layer's cell activations or outputs. Instead, we write explicit formulas defining the excitatory, E_{ij}, and inhibitory, I_{ij}, inputs to the membrane equations (2) that define cell activities within a particular layer. We also define the connection weights (or kernels) that specify the strength of excitation or inhibition delivered to a cell by other cells whose receptive field locations or orientational preferences bear fall within some (often Gaussian) tolerance zone. The activation equations for W_{ij} and for the rectified output signals V_{ij} of Eq. (2) are hereby completely defined for each model layer in turn.

We use the following index conventions. Location on a two-dimensional spatial grid and orientational preference, where appropriate, are specified by three subscripts, i, j, and k, respectively. The identity of a cell activation, W, or output value V—that is, the layer in the model to which a cell belongs—is coded by the following superscripts: R for retina, L for *LGN*, S1 for simple cells of layer 4 of V1, S2 for simple cells of opposite contrast polarity to those labeled S1, 3 for pyramidal cells of layer 2/3, 4 for "complex-like" cells of layer 4, and 6 for cells of layer 6. Inputs from ON and OFF retinal streams are coded by superscript plus, +, and minus, −, signs, respectively.

3.2. Retina

The retinal ON-cell (OFF-cell) activities and outputs are denoted, respectively, by W^{R+} (W^{R-}) and V^{R+} (V^{R-}), respectively. Retinal inputs and kernels also have a superscript "R" to denote the retina. The retinal parameters are given in Table 1. Once these parameters are determined, the retinal excitatory and inhibitory inputs fully define Eq. (2) for retinal activation. For the ON-cell activations W^{R+}, the narrow on-center is defined by:

$$E_{ij}^{R+} = S_{ij}, \tag{6}$$

and the broad off-surround is defined by:

$$I_{ij}^{R+} = \sum_{mn} S_{i+m,j+n} G_{mn}^{R}, \tag{7}$$

where the S_{ij} are the input image intensities, and G_{mn}^{R} is the unoriented Gaussian defined in Eq. (4); see Fig. 4A. The OFF-cell activations W^{R-} exhibit a broad on-surround:

$$E_{ij}^{R-} = \sum_{mn} S_{i+m,j+n} G_{mn}^{R}, \tag{8}$$

and a narrow off-center:

$$I_{ij}^{R-} = S_{ij}. \tag{9}$$

Parameters for retina. Eq. (3) combines biased DOG processing with a term that normalizes activity with a biased SOG in its denominator. This is just DOG/SOG processing with a relatively small value of A (see Table 1). The input gray levels were chosen between 0 and 255, but could have

Table 2
Cortical BCS parameters II

Name	Description	Value	Equation(s)
Stage II: V^{L} modeled LGN processing			
A	Activation decay rate	1.0	LGN shunt
B	Saturation level	1.0	LGN shunt
C	Hyperpolarization term	1.0	LGN shunt
σ_{L_c}	LGN center standard deviation	0.3	10
σ_{L_s}	LGN surround standard deviation	2.0	11

spanned a much wider dynamic range. See Neumann (1996) for a thorough analysis of the effects of parameter variations in such networks.

In our simulations of retinal cells (Eqs. (6)–(9)), parameters A, B, and C in Eq. (3) are set equal to 1.0 to balance the effects of excitatory and inhibitory kernels. This choice of parameters guarantees that any input region that has uniform values results in zero outputs, a property sometimes referred to as "featural noise suppression."

3.3. Lateral geniculate nucleus

The LGN ON-cell (OFF-cell) activities have a superscript L+ (L−). Their ON-cell and OFF-cell inputs from the retina have the superscript R+ or R−, while inputs from layer 6 have the superscript 6. Both center (L_c) and surround (L_s) unoriented LGN kernels $G^{L_c}_{mn}$ and $G^{L_s}_{mn}$ are used to define the interactions among these inputs in the LGN membrane equations. The LGN ON-cell activations W^{L+}_{ij} obey:

$$E^{L+}_{ij} = V^{R+}_{ij}\left(+ \sum_{mnk} V^{6}_{i+m,j+n,k} G^{L_c}_{mn}\right) \tag{10}$$

and

$$I^{L+}_{ij} = \sum_{mnk} V^{6}_{i+m,j+n,k} G^{L_s}_{mn}. \tag{11}$$

In Eq. (10), E^{L+}_{ij} describes how bottom-up retinal ON-cell output directly activates LGN, whereas on-center feedback from layer 6 can multiplicatively amplify this activation. In Eq. (11), I^{L+}_{ij} describes how off-surround feedback from layer 6 can broadly inhibit LGN ON-cell activity. The combined effect of these top-down terms is to select and synchronize LGN cells that receive both bottom-up retinal inputs and top-down layer 6 input, while inhibiting LGN cells that do not. In a similar fashion, the LGN OFF-cell activations W^{R-}_{ij} obey:

$$E^{L-}_{ij} = V^{R-}_{ij}\left(1 + \sum_{mnk} V^{6}_{i+m,j+n,k} G^{L_c}_{mn}\right) \tag{12}$$

and

$$I^{L-}_{ij} = \sum_{mnk} V^{6}_{i+m,j+n,k} G^{L_s}_{mn} \tag{13}$$

Parameters for LGN. The parameters for LGN processing are listed in Table 2. As with the retinal equations, A, B, and C in Eq. (3) were set equal to 1.0 to balance the effects of excitatory and inhibitory kernels.

3.4. Cortical area V1 (layer 4)

The V1 layer 4 activities W^{4}_{ij} receive oriented arrays of spatially displaced LGN ON and OFF cell outputs which excite mutually inhibitory simple cells that are sensitive to the same orientation but opposite contrast polarities. The oriented simple cell receptive fields are defined by the Gaussian kernel described in Eq. (5), where σ_{4l} and σ_{4w} represent the standard deviations of the length and width of the oriented simple cell kernels. In particular, each simple cell is excited by an oriented sample of LGN ON-cell output and excited by an adjacent and parallel oriented sample of the LGN OFF-cell output, as in Eqs. (14) and (15):

$$E^{S1}_{ijk} = \left(4 \sum_{mn} V^{L+}_{i+m,j+n,k} G^{4k+}_{mnk} + \sum_{mn} V^{L-}_{i+m,j+n,k} G^{4k-}_{mnk}\right)^2$$

$$E^{S2}_{ijk} = \left(4 \sum_{mn} V^{L+}_{i+m,j+n,k} G^{4k-}_{mnk} + \sum_{mn} V^{L-}_{i+m,j+n,k} G^{4k+}_{mnk}\right)^2$$

where each kernel G is defined by an oriented Gaussian; see Fig. 4B. The centers of these kernels are slightly offset from each simple cell's centroid directions along an axis perpendicular to the simple cell's direction of elongated sampling. In Eqs. (14) and (15), the oriented sample of the LGN ON-cell output was multiplied by a factor of 4 to compensate for the asymmetrical response of the on-center off-surround operators on opposite sides of an edge. To understand this asymmetry, consider the denominator of Eq. (3). On opposite sides of a bright-to-dark edge, the denominator varies greatly. Specifically, it is much smaller on the dark side of the edge. For this reason, at an edge, positive ON-cell signals are much weaker than adjacent positive OFF-cell signals. Oriented detectors driven by these asymmetrical ON/OFF responses show faster fall-off in response with distance on the bright side of an edge. This asymmetry complicates the problem of boundary sharpening using subsequent center–surround contrast enhancement. In particular, parameters which successfully sharpen the dark side of straight edges tend to suppress bright concave edges altogether. For the kernel sizes that we used, a factor of 4 compensated for this asymmetry, enabling a single inhibitory surround to sharpen the localization of boundary responses in many circumstances. After compensated ON and OFF cell oriented samplings were combined, the resulting simple cell activations were squared to exaggerate the response differences between weak and strong boundary responses. This sample non-linearity facilitated the subsequent competitive sharpening whereby strong boundary activities at edges inhibit surrounding boundary activations.

Simple cells of opposite polarity but of like orientation and location are then subtracted from each other and the two

Table 3
Cortical BCS parameters III

Name	Description	Value	Equation(s)
Stage III: V^4 modeled layer 4C processing			
A	Activation decay rate	1.0	Layer 4C shunt
B	Saturation level	1.0	Layer 4C shunt
C	Hyperpolarization term	2.0	Layer 4C shunt
σ_{4l}	Simple cell length standard deviation	2.4	5, (16, 17)
σ_{4w}	Simple cell width standard deviation	0.5	5, (16, 17)
Offset^{4+}	Simple cell ON offset	0.5	5, (16, 17)
Offset^{4-}	Simple cell OFF offset	−0.5	5, (16, 17)
σ_{L_m}	6-to-4 spatial standard deviation	4.0	5, (18)
σ_{L_o}	6-to-4 orientational standard deviation	45°	5, (18)

terms are rectified (Ferster et al., 1996; Gove et al., 1995; Liu, Gaska, Jacobson & Pollen, 1992). Finally, opposite polarity simple cells are additively combined to give a polarity-insensitive oriented cell activation E^C_{ijk} :

$$E^C_{ijk} = [E^{S1}_{ijk} - E^{S2}_{ijk}]^+ + [E^{S2}_{ijk} - E^{S1}_{ijk}]^+. \tag{16}$$

In vivo, layer 4 simple cells combine at layer 2/3 to drive complex cells. The simulations made the simplification of combining like-oriented but opposite polarity simple cells immediately as inputs to layers 4 and 6. This simplification makes the simulations computationally more tractable, by reducing the number of equations by a factor of 2, but does not affect performance on the polarity-insensitive boundary groupings which are simulated in this paper. For an unlumped treatment of simple-to-complex cell interactions, see Grossberg and McLoughlin (1997), Grunewald and Grossberg (1998), and McLoughlin and Grossberg (1998). In all,

$$E^4_{ijk} = E^C_{ijk} + V^6_{ijk} \tag{17}$$

and

$$I^4_{ijk} = \sum_{mno} V^6_{i+m,j+n,k+o} G^L_{mno} \tag{18}$$

are the total model excitatory and inhibitory signals to layer 4, which include on-center and off-surround inputs from layer 6; see Fig. 4C. The parameters are listed in Table 3.

V1, layer 4 parameters. The simple cells (Eqs. (14)–(16)) use a $C = 2.0$ parameter for the purposes of weighing the kernels in Eq. (3). This favors the inhibitory term in the simple cell activation equation, and allows sufficient boundary sharpening (i.e. suppression of spurious simple cell activity in regions with little image contrast) even with a large surround standard deviation, σ_{L_m}, of 4.0 and a standard deviation, σ_{L_o}, for orientational inhibition of 45°. The large spread of the surround cleans up boundaries in response to complex imagery. Simple cell size was chosen to fit the size of LGN center–surround receptive fields (see Fig. 4). However, varying the scales of the LGN and simple cells in proportion to each other would give similar performance.

3.5. Cortical area V1 (layer 2/3)

Layer 2/3 defines the long-range monosynaptic excitatory horizontal interactions and short-range disynaptic inhibitory interactions between pyramidal cells, whose activities are denoted by W^3_{ij}. Parameters β, μ, and λ in Eq. (26) below define the shape of the bipole kernel. Performance was insensitive to the exact values of these parameters. However, a small β gave sharper sensitivity to alignment between inducers, an intermediate μ made the bipole more tolerant of less than perfectly collinear alignment among inducers, and a large λ gave sharper orientational selectivity in completion choices. The layer 2/3 activations W^3_{ij} obey:

$$E^3_{ijk} = V^4_{ijk} + H^3_{ijk}, \tag{19}$$

where V^4_{ijk} defines the oriented input from layer 4 and H^3_{ijk} defines the total monosynaptic excitatory horizontal input. This horizontal input is composed of a short-range (s) and long-range (l) bipole signal:

$$H^3_{ijk} = h^s_{ijk} + h^l_{ijk}, \tag{20}$$

where

$$h^s_{ijk} = g \sum_{mno} f(V^3_{i+m,j+n,k+o}) Z_{20m/C_L,20n/C_W,o,k} \tag{21}$$

and

$$h^l_{ijk} = \sum_{mno} [V^3_{i+m,j+n,k+o} - T]^+ Z_{2m/C_L,2n/C_W,o,k} \tag{22}$$

Inhibition at layer 2/3 is driven by a recurrent spatial and orientation-sharpening term (V^3) and a term D that is driven disynaptically by the long-range bipole:

$$I^3_{ijk} = \sum_o V^3_{i,j,k+o} G^{3s}_o + D_{ijk}, \tag{23}$$

where

$$D_{ijk} : \; gf(h^l_{ijk})$$

with

$$f(w) = \frac{w}{\alpha + w}. \tag{25}$$

The horizontal interaction kernel that defines the bipole property in Eqs. (21) and (22) obeys

$$Z_{mnok} = \text{sgn}\{m\} \exp\{-\beta(m^2 + n^2)\} \exp\left\{-\mu\left(\frac{n}{m^2}\right)^2\right\} \times \cos^\lambda\left(\frac{(k-o)\pi}{K} - \text{sgn}\{m\} \arctan\left(\frac{2n}{m}, m\right)\right). \tag{26}$$

Eq. (26) gives rise to the types of oriented kernels shown in Fig. 4D and E, where the value of μ determines the tolerated deviation from strict collinearity. Variants of this kernel were introduced by Grossberg and Mingolla (1985) and

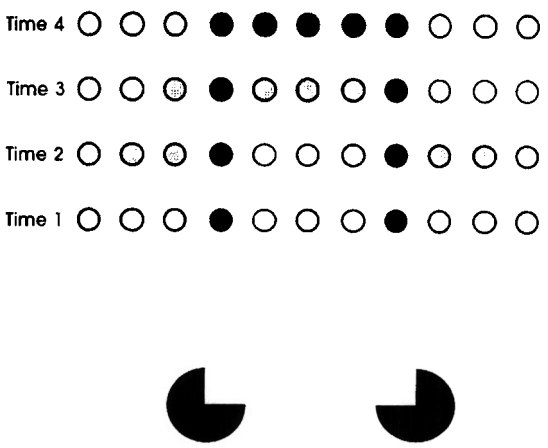

Fig. 5. Schematic of boundary completion in time. In response to the collinear edges of a Kanizsa square, layer 2/3 pyramidal cells first get activated at the positions of the edges (Time 1). A wave of activation then begins to spread in an oriented fashion in both directions to other pyramidal cells (Time 2). Cells at positions that lie outside the square are quickly inhibited by disynaptic inhibition (Time 3). Cells that lie between the edges can get strongly activated because the monosynaptic excitatory horizontal inputs are stronger than the total disynaptic inhibitory interneuronal inputs at these positions (Time 4).

later supported by many data, including those of Field et al. (1995), Polat and Sagi (1994), and Shipley and Kellman (1992). In the bipole signal function $f(w)$ in Eq. (25), α is set small to define a steep response. The inhibitory gain g in Eq. (24) is set so that the short-range excitatory bipole signal h^s in Eq. (21) must be maximally active to overcome the disynaptic inhibitory effect of D_{ijk}, which is a function of the long-range excitatory bipole signal h^l. This balance ensures that each active layer 2/3 pyramidal cell either receives direct bottom-up activation or that it falls on a collinear or slightly curvilinear path between two or more such cells.

In particular, initial exposure to an image spreads a transient monosynaptic pattern of boundary cell activation across layer 2/3 through the lateral excitatory connectivity H^3. Next, consider those cells where boundary activation was induced through lateral connectivity alone, and not through direct bottom-up activation—that is, any E^3 term where V^4 is zero in Eq. (19). At such locations, the long-range interaction h^l excites V^3 via Eq. (20) and then the short-range term h^s via Eq. (21). This short-range term h^s thereupon competes with the disynaptic inhibitory term D via Eqs. (20) and (23), respectively. At boundary activities that spread beyond rather than between inducers, the absence of strong enough short-range bipole activation results in suppression and the shrinking back of boundary activation toward inducers. Between pairs or greater numbers of inducers, short-range excitatory bipole activation overcomes disynaptic inhibition and a completed contour grows in strength in proportion to the contextual evidence.

Fig. 5 illustrates these ideas by showing how the dynamics of boundary completion can occur in response to a Kanizsa square. Initially, the pac man figures generate waves of excitation in both directions using the long-range horizontal connections. The short-range disynaptic inhibition quickly inhibits excitation outside the square, due to the one-against-one property. Within the square, however, the two-against-one property enables the long-range excitation to overcome the short-range disynaptic inhibition and form the illusory contour.

To understand the dynamics of the bipole mechanism, consider the time-course of the model's layer 2/3 response to boundary inducers. Initially, bottom-up excitation of layer 2/3 results in an activation of boundary cells representing the inducers. The activation pattern results from excitation described in Eq. (19) and is embodied in non-zero activity of layer 4 cells (V^4). At this point, boundary cells in layer 2/3 without bottom-up support from V^4 are inactive.

Next, the subset of these cells whose receptive field centers are collinear or slightly curvilinear—that is, "relatable" (Shipley & Kellman, 1992)—with boundary inducers and whose receptive fields include the inducers are activated through the influence of the long-range horizontal bipole cells, again through the excitation equation (19) but this time due to the horizontal component (H^3, see Eq. (20)) and specifically through the H^3 long-range term h^l (see Eq. (22)). At this point, layer 2/3 boundary activations are beginning to build at both interpolated and extrapolated boundary locations (see Fig. 5).

Next the influence of both disynaptic inhibition (D) and short-range bipole excitation (h^s) are engaged and the critical balance between these two acts to suppress extrapolated boundaries, in agreement with neuroanatomical and neurophysiological data suggesting that horizontal connections in layer 2/3 have both excitatory and inhibitory influences (Cannon & Fullenkamp, 1993; Hirsch & Gilbert, 1991; Knierim & van Essen, 1992; Somers et al., 1995; Stemmler et al., 1995). In the model, disynaptic inhibition is a saturating function of long-range bipole activation (h^l), as described in Eq. (24). Disynaptic inhibition is a steep function of (h^l), since $f(w)$ described in Eq. (25) is virtually a step function with α set very small. It should be noted that, from a computational perspective, disynaptic inhibition could also be driven by the short-range bipole activations (h^s), but no functional advantage is gained by including this additional connectivity.

In order to capture the disynaptic time-course of the inhibitory term D_{ijk}, the activity in layer 2/3 was calculated twice for each iteration of the layer 2/3 equations, each time using D_{ijk} from the previous time-step or iterative instant. The parameters are listed in Table 4.

VI, layer 2/3 parameters. The complex cells in layer 2/3 (Eqs. (3) and (19)–(26)) are more sensitive to parameter variations than the other cells in our model. First, the large A term (see Table 1) means that the activation equation (3) for this layer functions essentially as a DOG with little normalizing influence from the SOG in the denominator. Of course, the SOG normalization in earlier layers guarantees that activation at subsequent layers is always bounded and

Table 4
Cortical BCS parameters IV

Name	Description	Value	Equation(s)
Stage IV: V^3 modeled layer 3 processing			
A	Activation decay rate	2000.0	Layer 3 shunt
B	Saturation level	0.5	Layer 3 shunt
C	Hyperpolarization term	1.0	Layer 3 shunt
α	Non-linearity constant	0.0000001	$f(w)$
T	Bipole rule threshold	0.00001	22
G	Disynaptic inhibitory gain	2.0	24
C_L	Bipole length	10.0	21, 22
C_W	Bipole width	2.0	21,22
β	Distance blur	0.8	25
μ	Curvature blur	11	25
λ	Orientational blur	90	25

in a "known" range. This helped to implement the bipole property by using the difference between excitatory and inhibitory influences. The signal saturation constant α in Eq. (25) and the bipole threshold T in Eq. (22) were both set small to implement the bipole role. The disynaptic inhibition gain, g, was set equal to 2.0 in order to enforce suppression of boundaries extrapolated beyond edges rather than interpolated between them.

The parameters that implement the bipole property need to properly balance excitation and inhibition during the grouping process. The balance ensures three key outcomes at locations lacking direct "bottom-up" excitatory input: (1) interpolation, if that location is aligned with two or more other active cells with similar orientational preferences; (2) no extrapolation at cells that have such active neighbors on only one side; and (3) a proportionality of response, such that the strength of a completion signal is similar to the strength of supporting signals from nearby active cells.

We achieved these computational results as follows. The constant of 20 embedded in the spatial indices of Eq. (21) generates a functional "short-range" gating mechanism, which acts like a switch that allows a layer 2/3 cell to remain active only if its immediate collinear and like-oriented neighbors are also active, as explained below. The corresponding constant 2 in Eq. (22) allows longer-range "evidence gathering" in support of grouping to extend over several nearby lattice locations. The values 20 and 2 generate a 10–1 range of sizes for the effective kernels of these computations; other sizes could also have been used. We wrote 20 and 2 as opposed to 10 and 1 because doing so allows the bipole kernel Z in Eq. (26) to be written more simply. The indexing of Z is scaled by C_L and C_W in Eqs. (21) and (22) as a way of specifying bipole length and aspect ratio. Fig. 4D and E shows that the bipole kernels are narrow and biased along the positions that are aligned with the cell orientational preferences. Compare Fig. 24 of Gove et al. (1995) and Figs. 32 and 33 of Grossberg and Mingolla (1985) for variants of this bipole shape.

The inhibitory gain parameter, g in Eq. (24) is set to approximately balance short-range bipole activation due to h^1 in Eq. (20). Given the choice $g = 2.0$, it follows that the disynaptic inhibition (D) at any location receiving long-range bipole activation in Eq. (24) is nearly (i.e. close to, and just less than) 2.0.

Again for concreteness, assume that the spatial extent of the short-range bipole in Eq. (21) is three neural units, encompassing the boundary cell in question and a single boundary cell on either side of that cell. By "either side" is meant those locations "pointed to" by the orientational preference of the boundary cell in question. Thus, the relevant neighbors for a cell tuned to horizontal boundaries would be those cells whose receptive field centers are just to the left and just to the right of the cell in question. For a vertically tuned cell, the neighbors' receptive field centers would be just above and just below that of the cell in question, and so forth. When all three of these cells are activated, the short-range bipole of Eq. (21) achieves a value of 2.0.

This occurs because, in Eq. (21), the approximate step function $f(w)$ in Eq. (25) reaches full activation in response to the V^3 terms at the location of, and at locations on either side of, the boundary cell in question. In this case, the normalized bipole function (Z) is fully activated through multiplication with $f(V^3)$ at each bipole location and, after multiplication by g, the total activation of (h^s) approximates 1.0. Thus, for interpolated boundary activations, the disynaptic inhibition of 2.0 is cancelled out by the short-range bipole excitation of 2.0 and the excitatory influence of the long-range bipole can be expressed.

On the other hand, at the leading or outermost edge of extrapolated boundaries, the disynaptic inhibition is still 2.0, while the short-range bipole activation is only driven by two out of three bipole components and its activation has a lower value (approximately 1.5). At these locations, the disynaptic inhibition, D is not cancelled out by the short-range bipole, h^s, and D can suppress the smaller excitatory influence of the long-range bipole (h^l). By this mechanism, extrapolated boundaries are progressively pruned away and they retreat back to induced boundary cells, which are supported through bottom-up activation.

In summary, the disynaptic inhibition, D, should be strong enough to counteract excitation due to partial activation (in this case, two components) of the short-range bipole, h^s, plus any possible long-range bipole, h^l excitation. This can be ensured through a sufficiently large choice of the gain parameter, g, which scales both disynaptic inhibition and short-range bipole contributions in Eqs. (24) and (21), respectively. When this is accomplished, the system interpolates and does not extrapolate as follows: (1) bottom-up input results in an initial boundary activity at V^3 from V^4 simple cells in Eq. (19); (2) lateral excitation spreads across V^3 by way of h^l in Eq. (20), resulting in a non-zero H^3 that recurrently excites V^3 through Eq. (19); (3) short-range excitation and disynaptic inhibition acts through V^3 to h^s in Eq. (21) and H^3 in Eq. (20), and then via E^3 in Eq. (19); (4) disynaptic inhibition acts through h^l in Eq. (22) and D in

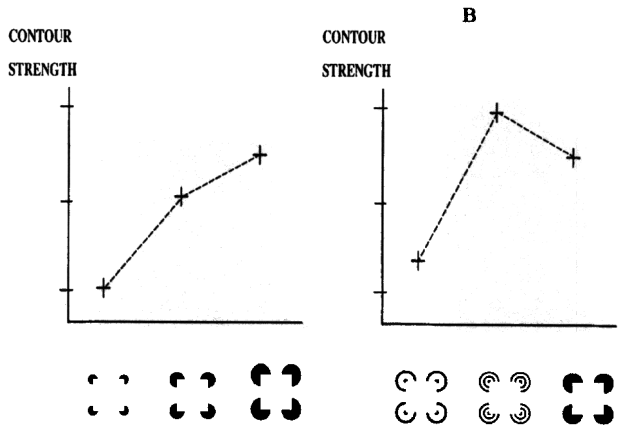

Fig. 6. Model simulations of psychophysical data. (A) In response to the edge inducers in Fig. 6A, illusory contour strength increases with support ratio. Support ratio is the ratio of real to total contour length. (B) For the line end inducers in Fig. 6B, contour strength is an inverted U function of the number and density of line end inducers. Contour strength was determined by computing the average cell activity in layer 2/3 along the path of the illusory portion of the contour. (Adapted with permission from Grossberg et al. (1997), Fig. 2).

Eq. (24) to I^3 in Eq. (23); and (5) wherever V^4 (Eq. (19)) is zero, it is the balance between excitation H^3 and inhibition D that determines whether induced boundary activation survives or is suppressed. Step four repeats until the extrapolated boundaries shrink back to boundaries supported by bottom-up activation. In other words, after an initial burst of long-range bipole excitation (h^1), cells must be surrounded on two sides by active boundary cells h^s, or they are suppressed by D.

3.6. Cortical area VI (layer 6)

Activity W^6_{ijk} was computed from a bottom-up oriented term that is assumed to come from LGN and a top-down term from layer 2/3. It was assumed that this term derives its oriented tuning by being associated with oriented signals from other cortical layers, including layers 4 and 2/3. For computational tractability, this term was approximated by E^C:

$$E^6_{ij} = 0.5E^C_{ijk} + V^3_{ijk}. \quad (27)$$

3.7. Cortical area V2

In the model of area V2 layers, the equations for the V1 layers 4, 2/3, and 6 were replicated with layer 2/3 from V1 forming the excitatory input to layers 4 and 6 in area V2. In area V2, the scale of horizontal bipole connectivity, in both length and width (parameters C_L and C_W in Table 4) were doubled, while all other parameters remained the same.

3.8. Simulation methods

In simulations of the model, equilibrium solutions at each processing level were calculated and the whole progression of levels was iterated until a convergence criterion was satisfied (between 2 and 5 iterations were typically needed). The convergence criterion specified that no activation level could change by more than 10% during the final iteration step. Sequential iteration of the equilibrium solutions of each stage reduced the simulation time. Comparisons with simulations of the full system as a set of differential equations verified that all the qualitative properties of the iterated solution held. The cortical loop was simulated in the following repeating cycle: LGN–6–4–2/3–6. Including the feedback to layer 6 after computing layer 2/3 ensured that the effects of internal cortical processing influenced the LGN via feedback from layer 6 on each cycle.

All Gaussian kernels in the model were truncated at plus and minus two standard deviations. To avoid spurious edge effects at the border of the image, the image was extended outwards for a distance corresponding to two standard deviations of the (larger) inhibitory retinal kernel.

4. Results

4.1. Boundary completion perpendicular to line ends

The model displays properties of spatial context-sensitivity by forming groupings that are either collinear with edges or perpendicular to line ends, depending upon the spatial arrangement of the input elements. A key property of such groupings is the sensitivity of their perceptual strength to contextual changes in stimulus properties. This sensitivity is illustrated by the following two properties. As the support ratio (namely, the ratio of real to total contour length) of a Kanizsa square increases, so too does the strength of the illusory contours that form between the square's pac man inducers (Shipley & Kellman, 1992). This property is stimulated in Fig. 6A. In addition, contour strength is an inverted U function of the number and density of line-end inducers of an illusory square (Lesher & Mingolla, 1993; Soriano, Spillman & Bach, 1996). This property is simulated in Fig. 6B. Such sensitivity to context suggests that the visual system is not merely computing independent measures of the likelihood or strength of local boundary orientations, but also evaluates the coherency of boundary groupings as well. Spatial context-sensitivity allows perceptual groupings to selectively bind together those image features—whether defined by edge, texture, shading, or stereo cues—that belong to the same objects in a scene. We call the property of analog-sensitive response to spatially distributed contextual evidence *analog coherence*. Such responses reflect more than just local stimulus energy. Instead, they are measures of the spatially distributed *coherent energy* for boundary likelihood or strength.

The sensitivity during feedforward processing to input contrast is due to the action of on-center off-surround network from layer 6-to-4. The preservation of contrast-

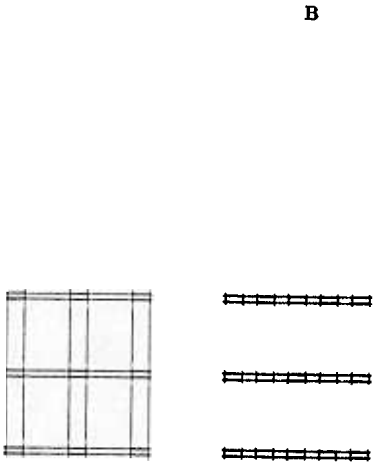

Fig. 7. (A) An ambiguous grouping (both vertical and horizontal) may be perceived in response to this image, and is simulated by the model. (B) Additional aligned horizontal items cause the grouping to become horizontal in perception and the model. (Adapted with permission from Grossberg et al. (1997), Fig. 6).

sensitivity when the feedback loop closes between layers 6–4–2/3–6 is due to the folded feedback that the loop activates. The increase in contour strength with support ratio in Fig. 6A is due to the cooperative action of increasing numbers of pyramidal cells on a shared target pyramidal cell in layer 2/3. The inverted U property in Fig. 6B is due to the fact that, as input density increases, each bottom-up input is attenuated more by layer 6-to-4 spatial inhibition before it can activate target pyramidal cells in layer 2/3. Thus, although there are more input sources, each one has a smaller effect on grouping by the layer 2/3 pyramidal cells.

4.2. Gestalt grouping

The analog sensitivity of grouping strength to the balance between these cooperative and competitive factors can be used to explain various Gestalt grouping laws. The Gestalt psychologists (e.g. Koffka, 1935; Wertheimer, 1923) proposed that perceptual grouping is the result of attractive field forces between stimulus elements. This Gestalt field theory did not survive, but the Gestaltists' demonstrations stimulated a great deal of additional empirical research and concept formation. The present cortical model exhibits a number of Gestalt properties without invoking fields.

In response to Fig. 7A (top), many observers perceive an ambiguous grouping in which both horizontal and vertical groupings coexist, the horizontal groupings joining the input elements within each row of the image, whereas the vertical groupings join the elements within each column. A similar organization is seen in Fig. 7A (bottom), which simulates the model's response to the input pattern in Fig. 7A (top). Fig. 7A (bottom) plots the simulated equilibrium values of the layer 2/3 complex cells in area V2 of the model. Placing

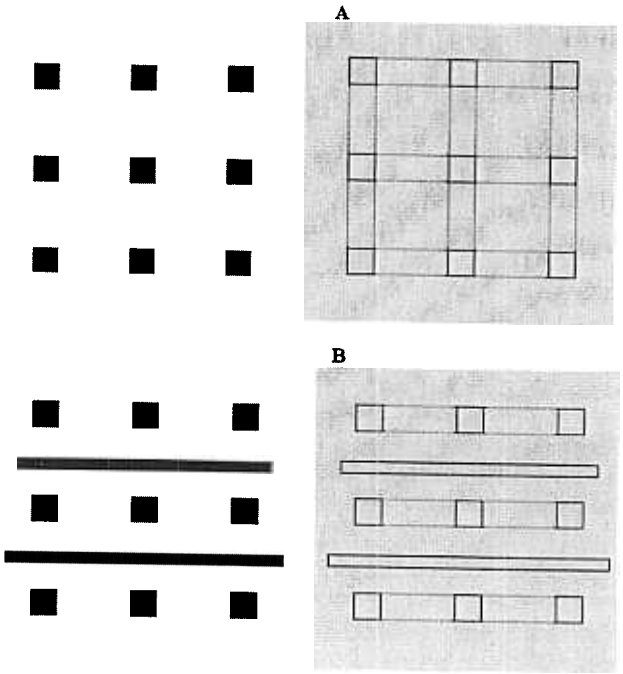

Fig. 8. (A) An ambiguous grouping (both vertical and horizontal) may be perceived in response to this image (left panel), and is simulated by the model (right panel). (B) The addition of horizontal bars blocking the vertical groupings causes the perceived and model groupings to become exclusively horizontal. Note: the perception of depth, a level of complexity not handled by the current version of our model, may restore the vertical groupings behind the bars (see Grossberg (1997) for a discussion of such factors).

additional elements within the rows of this figure, as in Fig. 7B (top) leads to an unambiguous percept of a horizontal grouping. A similar effect is seen in the model simulation of this grouping in Fig. 7B (bottom). This demonstration illustrates the Gestalt law of *proximity*. It results from the analog coherence of the horizontal and vertical boundary groupings. As more horizontal inducers are added in Fig. 7B, the horizontal grouping increases in strength in layer 2/3. This stronger grouping causes greater inhibition of the vertical grouping than conversely via layers 6 and 4.

Fig. 8 illustrates the Gestalt law of *good continuation*. In Fig. 8A, an ambiguous horizontal and vertical grouping is generated both perceptually and in the model simulation. In Fig. 8B, horizontal lines are interpolated between the square inducers. Now the vertical groupings are broken and the horizontal groupings are in the same direction as the horizontal lines. This effect again results from the context-sensitive interaction of long-range cooperation in layer 2/3 with shorter-range competition from layer 6 to 4 in the model.

4.3. Collinear cooperation and perpendicular competition in V1 and V2

It is known in vivo that cells in both V1 and V2 respond when illusory contours span closely spaced line ends

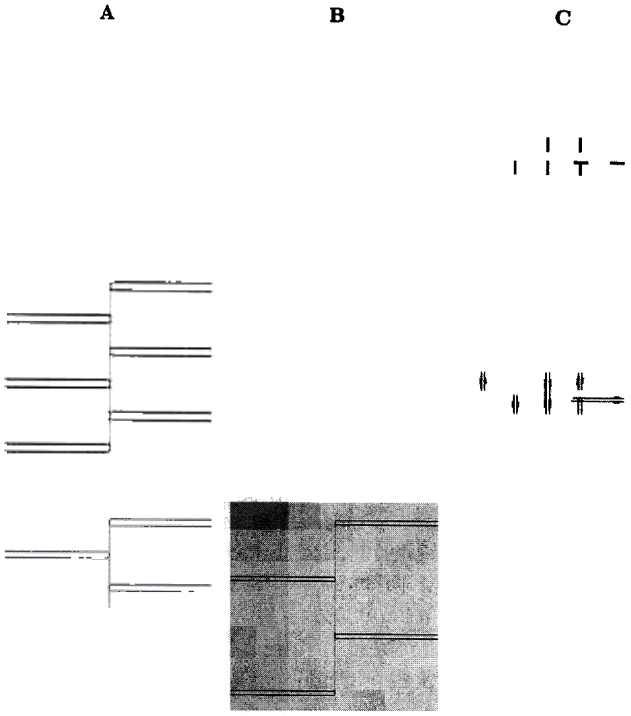

Fig. 9. Simulation of the: (A) Grosof et al. (1993) display—illusory contours between the offset gratings occur in both V1 and V2; (B) von der Heydt et al. (1984) display—illusory contours group the line ends in V2 but not V1; (C) Kapadia et al. (1995) display—horizontal orientations compete with the vertical grouping. The displays are in the top row, the simulated V1 responses are in the middle row, and the simulated V2 responses are in the bottom row. Kapadia et al. (1995) reported data only from V1. Note that the longer range of bipole interactions in V2, as opposed to V1—see Fig. 4D and E, respectively—accounts for the ability of the model to form the grouping of column B in V2 but not V1. (Adapted with permission from Grossberg et al. (1997), Fig. 4).

(Grosof et al., 1993; Redies, Crook & Creutzfelt, 1986), as shown in the simulation of Fig. 9A, which displays the equilibrium activities of layer 2/3 complex cells in areas V1 (middle row) and V2 (bottom row). On the other hand, cells in V1 do not respond when illusory contours span larger distances in response to thinner inducers, whereas cells in V2 do (von der Heydt et al., 1984; von der Heydt and Peterhans, 1989), as shown in the simulation of Fig. 9B. Within the model, these properties are due to the hypothesis that areas V1 and V2 share a similar organization, but that V2 can group over larger distances. As a result, both the shorter-range horizontal connections of V1 and the longer-range horizontal connections of V2 can group across the input elements in Fig. 9A, but only the longer-range connections of V2 can group across the more widely separated input elements in Fig. 9B.

Fig. 9C simulates data of Kapadia, Ito, Gilbert and Westheimer (1995) from monkey area V1 showing how perpendicular inducers can prevent groupings from occurring (see broken vertical grouping at the right hand side of the figure), even while groupings between collinear inducers form and improve stimulus detectability by mutual

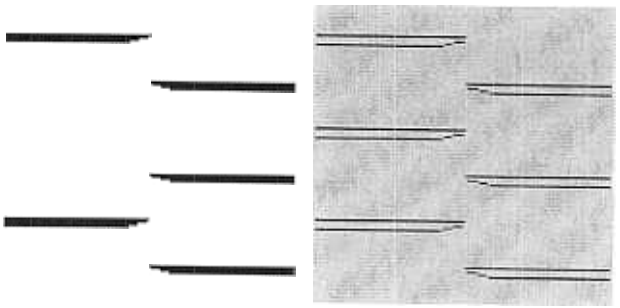

Fig. 10. Illusory contours form perpendicular to regular line ends (e.g. Fig. 8), but not perpendicular to pointed line ends, both in perception and in the model simulation.

activation (see stronger vertical activations in the middle of the figure than at its left hand side). In the model, the perpendicular competition is the V1 version of the V2 competition that broke the vertical grouping in Figs. 7B and 8B. The improved stimulus detectability is due to the sensitivity to collinear vertical groupings.

Not all aligned line ends can generate perpendicular groupings (Kennedy, 1978). In particular, line ends that come to a point cannot generate groupings as part of many configurations in which regular line ends can generate an offset grouping. This context-sensitive property is illustrated by the computer simulations in Fig. 10.

4.4. Signal-to-noise ratio enhancement and camouflage penetration

An interesting property of the model is its enhanced signal-to-noise ratio shown by the recovered measures of coherent orientational "energy"—that is, a consistent large-scale alignment of locally weak signals—using purely local boundary energy measurements. Fig. 11 illustrates this model property using a noise-degraded image. Fig. 11A shows the textured summation of cell activities E^C (see Eq. (16)) that results from a noise-degraded image of a dark square on a gray background. The square edge signals are camouflaged by noise. Fig. 11B shows how the model layer 2/3 horizontal cell grouping can select the boundaries out of the clutter, thereby enhancing the signal-to-noise ratio.

5. Discussion

The cortical model presented in this article suggests how the laminar, columnar, and map structures of cortical areas V1 and V2 are organized for the purposes of perceptual grouping. The model shows how distributed visual features can be coherently bound together through feedback interactions, without a loss of analog sensitivity. The model hereby suggests how the visual system measures the coherent spatially distributed evidence for a local visual feature's likelihood or strength, thereby computing a feature's coherent, rather than purely local, energy. The model describes

Fig. 11. (A) A noise-degraded image of a dark square on a gray background gives rise to textured summation of complex cell input strengths E^C in which the square edge signals are camouflaged by noise. (B) After processing by complex cells in layer 2/3, the coherent boundary signals emerge out of the clutter.

how the laminar organization of visual cortex is capable of realizing such processes through the use of the folded feedback pathway from the pyramidal cells in layer 2/3 back to layer 4 via layer 6. This feedback interaction helps to bind cortical cells into functional columns. The model also suggests how non-classical properties of cell receptive fields, such as their patch-suppressed responses (Born & Tootell, 1991; Sillito, Grieve, Jones Cudeiro & Davis, 1995), may arise through combining long-range horizontal grouping interactions in layer 2/3 with the shorter-range on-center off-surround interactions from layer 6-to-4, when these interactions are embedded within the cortical hypercolumn map.

Layer 6-to-4 inhibition may also contribute to the endstopping effect by which the responses of oriented cells to the middle portion of a long edge are attenuated relative to cell responses at edge ends or at short edges. Experimental studies of endstopping have used reversible inactivation of layer 6 in V1 using the inhibitory transmitter GABA. This manipulation causes cells in layer 4 to lose their end-inhibition, as well as cells in layer 2/3 that receive their inputs from layer 4 (Bolz & Gilbert, 1986; Bolz, Gilbert & Wiessel, 1989). An inhibitory interaction with a mean length of 2.8 degrees in cat cortical area V1 (area 17) has been reported (Grieve & Sillito, 1991), which matches well the value predicted for the inhibitory field that generates endstopping (Kato, Bishop & Orban, 1978; Sillito, 1977; Yamane, Maske & Bishop, 1985).

These data do not necessarily imply, however, that layer 6-to-4 inhibition is the only mechanism that influences endstopping. In particular, corticogeniculate feedback, which also exhibits a center–surround organization, may also indirectly influence endstopping (Murphy & Sillito, 1987). In the model, feedback from layer 6 cells to the LGN enhances LGN cell responses near line ends, thereby strengthening the perpendicular cortical responses at line ends that enable the corresponding cortical cells to group cooperatively, as in the simulations of Figs. 6B and 7A.

Reversible inactivation of layer 6 in V1 using GABA (Bolz & Gilbert, 1986; Bolz et al., 1989) does not substantially change orientational selectivity of cells in visual cortex. The same is true in the model, due to the fact that the excitatory inputs to layer 4C model cells are already orientationally tuned.

The possible role of layer 6-to-4 inhibition in endstopping has been questioned because layer 6 connectivity also enhances the excitability of non-length-tuned cells in layers 2/3 and 4 (Grieve & Sillito, 1995). The model proposes that this interaction is, more generally, part of the mechanism that ensures analog coherence of cortical processing, namely, it helps to preserve contrast-sensitivity to inputs from the LGN and helps to select correct groupings in response to feedback from layer 2/3, without a loss of sensitivity to feature contrast or spatial context. Various other cortical models (e.g. Douglas et al., 1995; Grossberg, 1976a,b; Heeger, 1993; Olson and Grossberg, 1998; Somers et al., 1995; Stemmler et al., 1995; Willshaw & von der Malsburg, 1976) have discussed the possible role of recurrent interactions in visual cortex. Neumann and Sepp (1999) have proposed a related model of V1 and V2 processing, which explores the role of recurrent long-range completion mechanisms, but does not address the laminar structure of these cortices. None of these models have yet modeled how cortical layers and their interactions control the formation of perceptual groupings that preserve their analog coherence under a wide range of stimulus conditions. The present articles begins to close this gap.

Acknowledgements

The authors wish to thank Robin Amos and Diana Meyers for their valuable assistance in the preparation of the manuscript. W.D.R. was supported in part by the Air Force Office of Scientific Research (AFOSR 90-0175), British Petroleum (BP 89A-1204), the Defense Advanced Research Projects Agency and the Office of Naval Research (ONR N00014-92-J-4015), HNC Software (SC-94-001), the National Science Foundation (NSF IRI-90-00530), and the Office of Naval Research (ONR N00014-91-J4100 and ONR N00014-95-1-0409). S.G. was supported in part by the Defense Advanced Research Projects Agency and the Office of Naval Research (ONR N00014-1-009 and the Office of Naval Research (ONR N00014-95-1-0657). E.M. was supported in part by the Defense Advanced Research Projects Agency and the Office of Naval Research (ONR N00014-95-1-0409).

References

Amir, Y., Harel, M., & Malach, R. (1993). Cortical hierarchy reflected in the organization of intrinsic connections in macaque monkey visual cortex. *Journal of Comparative Neurology, 334*, 19–46.

Beck, J., Prazdny, K., & Rosenfeld, A. (1983). A theory of textural segmentation. In J. Beck, B. Hope & A. Rosenfeld, *Human and machine vision*. New York: Academic Press.

Blasdel, G. G. (1992a). Differential imaging of ocular dominance and

orientation selectivity in monkey striate cortex. *Journal of Neuroscience, 12*, 3115–3138.

Blasdel, G. G. (1992b). Orientation selectivity, preference, and continuity in monkey striate cortex. *Journal of Neuroscience, 12*, 3139–3161.

Blasdel, G. G., & Salama, G. (1986). Voltage-sensitive dyes reveal a modular organization in monkey striate cortex. *Nature, 321*, 579–585.

Bolz, J., & Gilbert, C. D. (1986). Generation of end-inhibition in the visual cortex via interlaminar connections. *Nature, 320*, 362–365.

Bolz, J., Gilbert, C. D., & Wiesel, T. N. (1989). Pharmacological analysis of cortical circuitry. *Trends in Neurosciences, 12*, 292–296.

Bonhoeffer, T., & Grinvald, A. (1991). Iso-orientation domains in cat visual cortex are arranged in pinwheel-like patterns. *Nature, 353*, 429–431.

Born, R. T., & Tootell, R. B. H. (1991). Spatial-frequency tuning of single units in macaque supragranular striate cortex. *Proceedings of the National Academy of Sciences, USA, 88*, 7071–7075.

Bosking, W., Zhang, Y., Schofield, B., & Fitzpatrick, D. (1997). Orientation selectivity and the arrangement of horizontal connections in tree shrew striate cortex. *Journal of Neuroscience, 17* (6), 2112–2127.

Cannon, M. W., & Fullenkamp, S. C. (1993). Spatial interactions in apparent contrast: individual differences in enhancement and suppression effects. *Vision Research, 33*, 1685–1695.

Chapman, B., Zahs, K. R., & Stryker, M. P. (1991). Relation of cortical cell orientation selectivity to alignment of receptive fields of the geniculocortical afferents that arborize within a single orientation column in ferret visual cortex. *Journal of Neuroscience, 11*, 1347–1358.

Cohen, M. A., & Grossberg, S. (1984). Neural dynamics of brightness perception: features, boundaries, diffusion, and resonance. *Perception and Psychophysics, 36*, 428–456.

Douglas, R. J., Koch, C., Mahowald, M., Martin, K. A. C., & Suarez, H. H. (1995). Recurrent excitation in neocortical circuits. *Science, 269*, 981–985.

van Essen, D. C., & Maunsell, J. H. R. (1983). Hierarchical organization and functional streams in the visual-cortex. *Trends in Neurosciences, 6*, 370–375.

Felleman, D. J., & van Essen, D. C. (1991). Distributed hierarchical processing in the primate cerebral cortex. *Cerebral Cortex, 1*, 1–47.

Ferster, D. (1988). Spatially opponent excitation and inhibition in simple cells of the cat visual cortex. *Journal of Neuroscience, 8*, 1172–1180.

Ferster, D., & Lindström, S. (1983). An intracellular analysis of geniculocortical connectivity in area 17 of the cat. *Journal of Physiology, 342*, 181–215.

Ferster, D., & Lindström, S. (1985). Synaptic excitation of neurons in area 17 of the cat by intracortical axon collaterals of cortico-geniculate cells. *Journal of Physiology, 367*, 233–252.

Ferster, D., Chung, S., & Wheat, E. (1996). Orientation selectivity of thalamic input to simple cells of cat visual cortex. *Nature, 380*, 249–252.

Field, D. J., Hayes, A., & Hess, R. F. (1993). Contour integration by the human visual-system—evidence for a local association field. *Vision Research, 33* (2), 173–193.

Gilbert, C. D., & Wiesel, T. N. (1979). Brain mechanisms of vision. *Nature, 280*, 120–125.

Gove, A., Mingolla, E., & Grossberg, S. (1995). Brightness perception, illusory contours, and corticogeniculate feedback. *Visual Neuroscience, 12*, 1027–1052.

Grieve, K. L., & Sillito, A. M. (1991). The length summation properties of layer VI cells in the visual cortex and hypercomplex cell end zone inhibition. *Experimental Brain Research, 84*, 319–325.

Grieve, K. L., & Sillito, A. M. (1995). A re-appraisal of the role of layer VI of the visual cortex in the generation of cortical end inhibition. *Experimental Brain Research, 104*, 12–20.

Grinvald, A., Lieke, E. E., Frostig, R. D., & Hildesheim, R. (1994). Cortical point-spread function and long-range lateral interactions revealed by real-time optical imaging of macaque monkey primary visual cortex. *Journal of Neuroscience, 14* (15), 2545–2568.

Grosof, D. H., Shapley, R. M., & Hawken, M. J. (1993). Macaque V1 neurons can signal "illusory" contours. *Nature, 365*, 550–552.

Grossberg, S. (1973). Contour enhancement, short term memory, and constancies in reverberating neural networks. *Studies in Applied Mathematics, 52*, 217–257.

Grossberg, S. (1976a). Adaptive pattern classification and universal recoding, I: parallel development and coding of neural feature detectors. *Biological Cybernetics, 23*, 121–134.

Grossberg, S. (1976b). Adaptive pattern classification and universal recoding, II: feedback, expectation, olfaction, and illusions. *Biological Cybernetics, 23*, 187–202.

Grossberg, S. (1980). How does a brain build a cognitive code? *Psychological Review, 87*, 1–51.

Grossberg, S. (1984). Outline of a theory of brightness, color, and form perception. In E. Degreef & J. van Buggenhaut, *Trends in Mathematical Psychology* (pp. 59–86). Amsterdam: Elsevier/North-Holland.

Grossberg, S. (1987). Cortical dynamics of three-dimensional form, color, and brightness perception, I: monocular theory. *Perception and Psychophysics, 41*, 87–116.

Grossberg, S. (1994). 3-D vision and figure–ground separation by visual cortex. *Perception and Psychophysics, 55*, 48–120.

Grossberg, S. (1997). Cortical dynamics of three-dimensional figure–ground perception of two-dimensional pictures. *Psychological Review, 104*, 618–658.

Grossberg, S. (1999). How does the cerebral cortex work? Learning, attention, and grouping by the laminar circuits of visual cortex. *Spatial Vision, 12*, 163–185.

Grossberg, S., & McLoughlin, E. (1997). Cortical dynamics of 3-D surface perception: binocular and half-occluded scenic images. *Neural Networks, 10*, 1583–1605.

Grossberg, S., & Mingolla, E. (1985). Neural dynamics of perceptual grouping: textures, boundaries, and emergent segmentations. *Perception and Psychophysics, 38*, 141–171.

Grossberg, S., Mingolla, E., & Ross, W. D. (1997). Visual brain and visual perception: how does the cortex do perceptual grouping? *Trends in Neurosciences, 20*, 106–111.

Grunewald, A., & Grossberg, S. (1998). Self-organization of binocular disparity tuning by reciprocal corticogeniculate interactions. *Journal of Cognitive Neuroscience, 10*, 199–215.

Heeger, D. J. (1993). Modeling simple-cell direction selectivity with normalized, half-squared, linear operators. *Journal of Neurophysiology, 71*, 2543–2547.

von der Heydt, R., & Peterhans, E. (1989). Mechanisms of contour perception in monkey visual cortex. I. Lines of pattern discontinuity. *Journal of Neuroscience, 9*, 1731–1748.

von der Heydt, R., Peterhans, E., & Baumgartner, G. (1984). Illusory contours and cortical neuron responses. *Science, 224*, 1260–1262.

Hirsch, J. A., & Gilbert, C. D. (1991). Synaptic physiology of horizontal connections in the cat visual cortex. *Journal of Neuroscience, 11*, 1800–1809.

Hodgkin, A. L. (1964). *The conduction of the nervous impulse*, Liverpool, UK: Liverpool University.

Hubel, D. H., & Wiesel, T. N. (1962). Receptive fields and functional architecture of monkey striate cortex. *Journal of Physiology, 160*, 106–154.

Hubel, D. H., & Wiesel, T. N. (1977). Functional architecture of macaque monkey visual cortex. *Proceedings of the Royal Society of London (B), 198*, 1–59.

Julesz, B. (1971). *Foundations of cyclopean perception*, Chicago, IL: University of Chicago Press.

Kapadia, M. K., Ito, M., Gilbert, C. D., & Westheimer, G. (1995). Improvement in visual sensitivity by changes in local context: parallel studies in human observers and in V1 of alert monkeys. *Neuron, 15*, 843–856.

Kato, H., Bishop, P. O., & Orban, G. A. (1978). Hypercomplex and simple/complex cell classifications in cat striate cortex. *Journal of Neurophysiology, 41*, 1071–1096.

Kennedy, J. M. (1978). Illusory contours and the ends of lines. *Perception, 7*, 605–607.

Kisvarday, Z. K., Toth, E., Rausch, M., & Eysel, U. T. (1995). Comparison

of lateral excitatory and inhibitory connections in cortical orientation maps of the cat. *Society for Neuroscience Abstracts, 21*, 907.

Knierim, J. J., & van Essen, D. C. (1992). Neuronal responses to static texture patterns in area V1 of the alert macaque monkey. *Journal of Neurophysiology, 67*, 961–980.

Koffka, K. (1935). *Principles of Gestalt psychology*, New York: Harcourt, Brace and Jovanovich.

Lesher, G. (1995). Illusory contours: toward a neurally based perceptual theory. *Psychonomic Bulletin and Review, 2(3)*, 279–321.

Lesher, G. W., & Mingolla, E. (1993). The role of edges and line-ends in illusory control formation. *Vision Research, 33*, 2253–2270.

LeVay, S., Connolly, M., Houde, J., & Van Essen, D. (1985). The complete pattern of ocular dominance stripes in the striate cortex and visual field of the macaque monkey. *Journal of Neuroscience, 5*, 476–591.

Liu, Z., Gaska, J. P., Jacobson, L. D., & Pollen, D. A. (1992). Interneuronal interaction between members of quadrature phase and anti-phase pairs in the cat's visual cortex. *Vision Research, 32*, 1193–1198.

McClurkin, J. W., Optican, L. M., & Richmond, B. J. (1994). Cortical feedback increases visual information transmitted by monkey parvocellular lateral geniculate nucleus neurons. *Visual Neuroscience, 11*, 601–617.

McGuire, B. A., Gilbert, C. D., Rivlin, P. K., & Wiesel, T. N. (1991). Targets of horizontal connections in macaque primary visual cortex. *Journal of Comparative Neurology, 305*, 370–392.

McLoughlin, N. P., & Grossberg, S. (1998). Cortical computation of stereo disparity. *Vision Research, 38*, 91–99.

Mountcastle, V. B. (1957). Modality and topographic properties of single neurons of cats somatic sensory cortex. *Journal of Neurophysiology, 20*, 408–434.

Murphy, P. C., & Sillito, A. M. (1987). Corticofugal feedback influences the generation of length tuning in the visual pathway. *Nature, 329*, 727–729.

Murphy, P. C., & Sillito, A. M. (1996). Functional morphology of the feedback pathway from area 17 of the cat visual cortex to the lateral geniculate nucleus. *Journal of Neuroscience, 16*, 1180–1192.

Neumann, H. (1996). Mechanisms of neural architecture for visual contrast and brightness perception. *Neural Networks, 9* (6), 921–936.

Neumann, H., & Sepp, W. (1999). Recurrent V1–V2 interaction in early visual boundary processing. *Biological Cybernetics, 81*, 425–444.

Olson, S. J., & Grossberg, S. (1998). A neural network model for the development of simple and complex cell receptive fields within cortical maps of orientation and ocular dominance. *Neural Networks, 11*, 189–208.

Polat, U., & Sagi, D. (1994). The architecture of perceptual spatial interactions. *Vision Research, 34*, 73–78.

Ramachandran, V. S., & Nelson, J. I. (1976). Global grouping overrides point-to-point disparities. *Perception, 5*, 125–128.

Redies, C., Crook, J. M., & Creutzfeldt, O. D. (1986). Neural responses to borders with and without luminance gradients in cat visual cortex and dLGN. *Experimental Brain Research, 61*, 469–481.

Reid, R. C., & Alonso, J. -M. (1995). Specificity of monosynaptic connections from thalamus to visual cortex. *Nature, 378*, 281–284.

Schmidt, K. E., Goebel, R., Lowel, S., & Singer, W. (1997). The perceptual grouping criterion of collinearity is reflected by anisotropies of connections in the primary visual cortex. *European Journal of Neuroscience, 9*, 1083–1089.

Shipley, T. F., & Kellman, P. J. (1992). Strength of visual interpolation. *Perception and Psychophysics, 52*, 97–106.

Sillito, A. M. (1977). Inhibitory processes underlying the directional specificity of simple, complex, and hypercomplex cells in the cat's visual cortex. *Journal of Physiology, 271*, 699–720.

Sillito, A. M., Jones, H. E., Gerstein, G. L., & West, D. C. (1994). Feature-linked synchronization of the thalamic relay cell firing induced by feedback from the visual cortex. *Nature, 369*, 479–482.

Sillito, A. M., Grieve, K. L., Jones, H. E., Cudeiro, J., & Davis, J. (1995). Visual cortical mechanisms detecting focal orientation discontinuities. *Nature, 378*, 492–496.

Somers, D. C., Nelson, S. B., & Sur, M. (1995). An emergent model of orientation selectivity in cat visual cortical simple cells. *Journal of Neuroscience, 15*, 5448–5465.

Soriano, M., Spillman, L., & Bach, M. (1996). The abutting grating illusion. *Vision Research, 36*, 109–116.

Stemmler, M., Usher, M., & Niebur, E. (1995). Lateral interactions in primary visual cortex: a model bridging physiology and psychophysics. *Science, 269*, 1877–1880.

Weber, A. J., Kalil, R. E., & Behan, M. (1989). Morphology of single, physiologically identified retinogeniculate Y-cell axons in the cat following damage to visual cortex at birth. *Journal of Comparative Neurology, 289*, 156–164.

Wertheimer, M. (1923). Untersuchungen yur Lehre von der Gestalt. II. *Psychologische Forschung, 4*, 301–350.

Willshaw, D. J., & von der Malsburg, C. (1976). How patterned neural connections can be set up by self-organization. *Proceedings of the Royal Society of London (B), 194*, 431–445.

Yamane, S., Maske, R., & Bishop, P. O. (1985). Direction selectivity of simple cells in cat striate cortex to moving light bars: relation to moving dark bar responses. *Experimental Brain Research, 60*, 200–203.